

Research Paper

Cite this article: Mattsson M, Buisman K, Kuylenstierna D (2024) Modeling of intermodulation in a loaded-line phase shifter based on a polynomial varactor model. *International Journal of Microwave and Wireless Technologies*, 1–12. <https://doi.org/10.1017/S175907872400076X>


Received: 21 November 2023

Revised: 11 July 2024

Accepted: 22 July 2024

Corresponding author: Martin Mattsson;
Email: martin.mattsson@chalmers.se

Modeling of intermodulation in a loaded-line phase shifter based on a polynomial varactor model

Martin Mattsson¹ , Koen Buisman^{1,2} and Dan Kuylenstierna¹

¹Department of Microtechnology and Nanoscience, Chalmers University of Technology, Gothenburg, Sweden and ²Department of Electrical and Electronic Engineering, Advanced Technology Institute, University of Surrey, Surrey GU2 7XH, U.K.

Abstract

This paper investigates if there is an optimum design of loaded-line phase shifters with respect to phase shift/loss figure of merit (FOM) and linearity. The investigation was performed by comparing six loaded-line phase shifters that were implemented in printed circuit board (PCB) technology with shunt-loaded hyperabrupt varactor-diodes. It was demonstrated that the hyperabrupt varactor's C-V characteristics must be modeled with high accuracy to predict the nonlinear behavior. A polynomial varactor model was employed and experimentally validated. To extend the range of investigated parameter values, the extracted model was scaled and evaluated further in a circuit simulator. The investigation reveals that for a given varactor-capacitance, the phase shift/loss FOM is improved if the varactor-capacitance is evenly distributed and the unit cell length is much shorter than a quarter wavelength. The study demonstrates that the phase shift/loss depends mainly on the distribution of varactor-capacitance and Q factor. The intermodulation (IM) distortion is primarily proportional to the total varactor-capacitance per unit cell. The study also revealed that an increase in the varactor's Q factor results in higher IM. Therefore, it is a trade-off between low loss and low IM.

Introduction

Tunable phase shifters are key components in many applications, such as delayed-locked loops [1] and phased-array antennas used in communication and radar systems. The main function of a tunable phase shifter is to modify the phase shift or group delay of the transmitted signal with the smallest loss possible. Various phase-shifter topologies have been evaluated, e.g., switched-line phase shifters, hybrid-coupled reflection-type phase shifters [2–4], and loaded-line phase shifters [5–8]. Only the two latter may be used for analogue tuning and loaded-line phase shifters have advantages due to ease of implementation and relatively low loss if moderate orders of phase shift are needed [9].

Common for all phase shifter topologies, they include a tuning element to adjust the phase. Different tuning mechanisms, e.g., mechanical, magnetic, or electronic, have been evaluated. In many modern applications, e.g., active electronically steerable arrays, only electronic steering is relevant. In the past, exotic tuning mechanisms such as ferroelectric varactors have been evaluated for low loss with promising results [10, 11]. However, for ease of manufacturing, compatibility with active components technology, and still very competitive performance, semiconductor varactor diodes are still the most commonly used [6].

Besides introducing desired tunability in the phase shift, the nonlinear component will also add unwanted intermodulation (IM) distortion (IMD) of signals in the system, which may influence performance on system level, e.g., a degraded lobe pattern when used in active phased array antennas [12]. The input third-order intercept point (*IIP3*) is employed to characterize the linearity of a phase shifter. One contribution is for a phase shifter based on high-breakdown voltage ferroelectric varactors [13] and another for a micro-electromechanical systems (MEMS) based phase shifter [14], and in [15], it is presented for a variable-phase all-pass network implemented in BiCMOS. However, the *IIP3* is presented as a performance metric, and neither models nor methods are presented for optimizing trade-offs between phase-shift/loss figure of merit (FOM) and linearity.

In this paper, we report on a method for prediction of IMD in a loaded-line phase shifter using hyperabrupt semiconductor varactors as tuning elements. The method is demonstrated for a phase shifter based on the same design principle as presented in [7], but here with a significantly more in-depth analysis, a more accurate varactor-diode model, and nonlinear distortion simulations. The nonlinear simulations are based on a polynomial varactor model [16] and the harmonic balance method. The model is applied for optimization

© The Author(s), 2024. Published by Cambridge University Press in association with The European Microwave Association. This is an Open Access article, distributed under the terms of the Creative Commons Attribution licence (<http://creativecommons.org/licenses/by/4.0>), which permits unrestricted re-use, distribution and reproduction, provided the original article is properly cited.

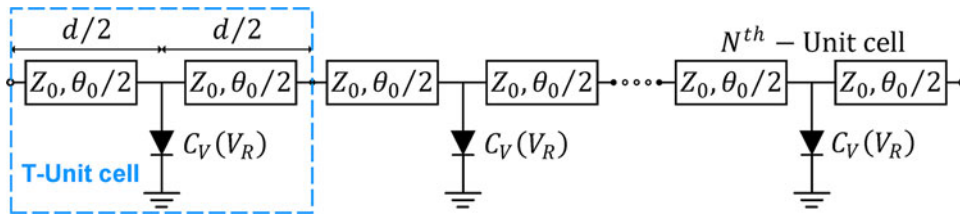


Figure 1. Illustration of the periodic loaded-line phase shifter with N number of T-unit cells.

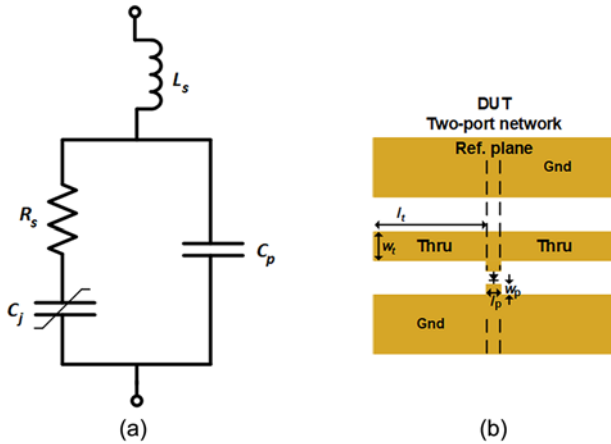


Figure 2. (a) Equivalent circuit model of reversed bias varactor-diode. The extracted values are $L_s = 1.51$ nH and $R_s = 1.49$ Ω , where the polynomial coefficients of $C_V = C_j + C_p$ are presented in Table 1. For comparison, the datasheet values are $L_s = 0.7$ nH, $R_s = 1.2$ Ω , $C_p = 0.81$ pF, and C_j is solved by (8) with $C_{j0} = 4.21$ pF, $\phi = 11.87$ V, and $n = 6.43$. (b) Illustration of two-port network employed to extract varactor parameters. Pad dimensions are $l_p = 0.5$ mm and $w_p = 0.4$ mm. Thru line dimensions are $l_t = 8$ mm and $w_t = 1.183$ mm.

Table 1. Values of the polynomial coefficients utilized to model the varactor's C-V characteristics

Coeff.	Value	Coeff.	Value
C_0	4.98E-12	C_{12}	8.19E-18
C_1	3.24E-12	C_{13}	5.47E-19
C_2	2.96E-12	C_{14}	2.85E-20
C_3	2.83E-12	C_{15}	1.15E-21
C_4	2.17E-12	C_{16}	3.50E-23
C_5	1.23E-12	C_{17}	7.80E-25
C_6	5.11E-13	C_{18}	1.20E-26
C_7	1.58E-13	C_{19}	1.13E-28
C_8	3.65E-14	C_{20}	4.99E-31
C_9	6.49E-15	C_{21}	1.20E-26
C_{10}	8.95E-16	C_{22}	1.13E-28
C_{11}	9.66E-17	C_{23}	4.99E-31

of the trade-off between linearity and phase-shift/loss FOM. The simulations are further used to investigate how different design factors, e.g., periodicity and varactor inclusion factor, affect the phase shift performance. Specifically, it is investigated how the performance of the phase shifter varies with input power, bias condition, periodicity, number of unit cells, and varactor-capacitance per unit length.

The rest of this paper is organized as follows. Section “Theory” presents the theoretical background on how to design a loaded line phase shifter optimized for phase-shift/loss FOM. Section

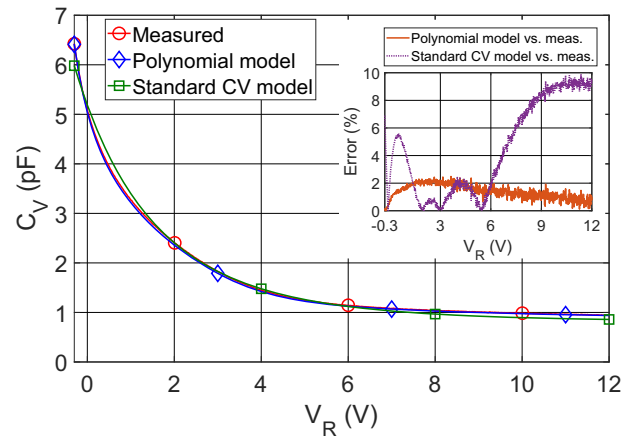


Figure 3. The C-V characteristic of the measured data, polynomial model and the standard C_V model. The inset depicts the relative error between the measured data and the two models.

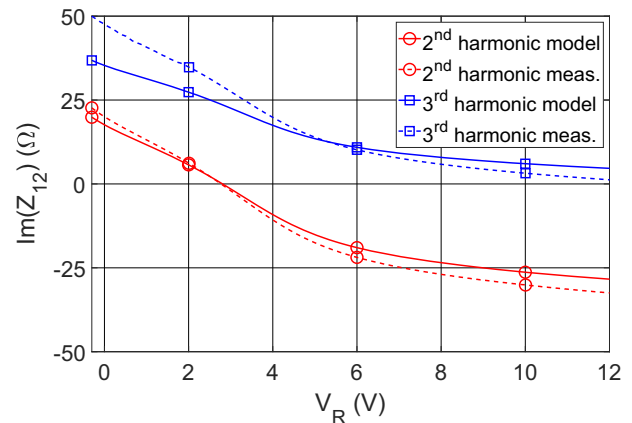


Figure 4. Modeled and measured $\text{Im}(Z_{12})$ for the second harmonic (3 GHz) and third harmonic (4.5 GHz).

“Phase shifter design” presents the design of the phase shifter including nonlinear varactor modeling. Then, Section “Nonlinear phase shifter simulations” presents nonlinear simulations. Section “Experimental results” presents experimental validation of the model. In Section “Model based optimization”, the developed model is applied to investigate how a loaded-line phase shifter can be simultaneously optimized for best possible trade-off between phase shift and linearity. Finally, Section “Conclusion” concludes this work.

Theory

Loaded-line phase shifter

A loaded-line phase shifter is composed of a transmission line periodically loaded by shunt-susceptances. Varactor-diodes are

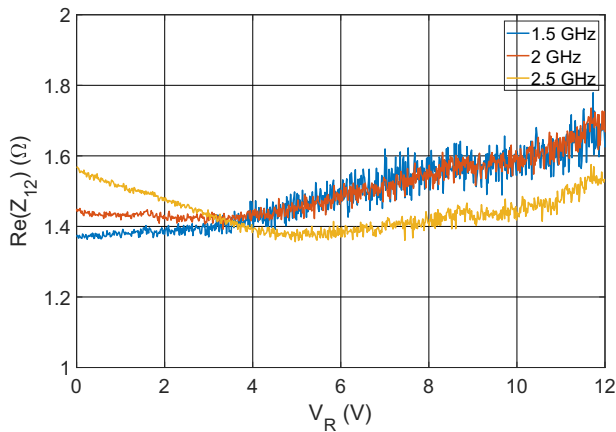


Figure 5. Real part of the measured varactor impedance.

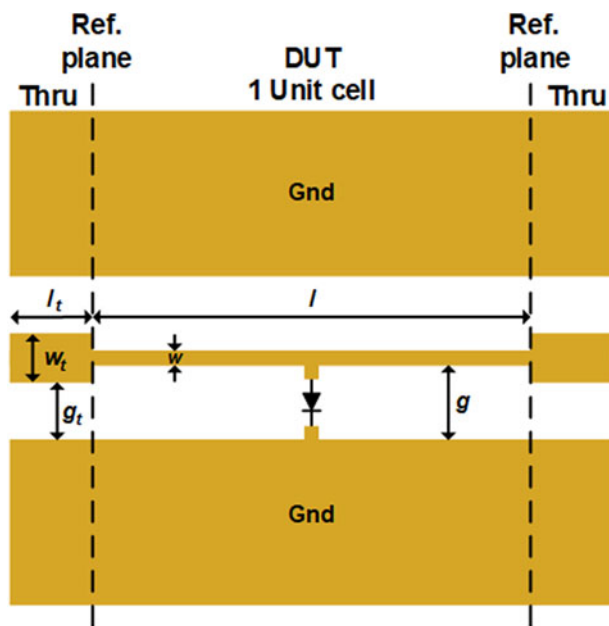


Figure 6. Illustration of the unit cell configuration composed of the unit cell and the thru lines. The dimensions of the unit cell with $\theta_e = 57.7^\circ$ are $l = 10.1$ mm, $w = 0.31$ mm, and $g = 2.34$ mm. The dimensions of the unit cell with $\theta_e = 66.4^\circ$ are $l = 13.14$ mm, $w = 0.4$ mm, and $g = 2.29$ mm. The dimensions of the thru line are $l_t = 8$ mm, $w_t = 1.183$ mm, and $g_t = 1.9$ mm.

commonly employed as the loading, as depicted in Fig 1. In the illustration, there is a T-unit cell (UC) that consists of two transmission lines of length $d/2$, and with a shunt-loaded varactor diode in between. The transmission line has an inductance per unit cell length L_t and a capacitance per unit cell length C_t . The varactor-diode has a voltage-controlled capacitance $C_V(V_R)$, where V_R is the reversed bias voltage. The transmission line has an unloaded impedance Z_0 , and the effective characteristic impedance Z_e of the unit cell can be expressed as

$$\begin{aligned}
 Z_e &= \sqrt{\frac{L_t}{C_t + C_V(V_R)/d}} \\
 &= \sqrt{\frac{L_t}{C_t}} \times \frac{1}{\sqrt{1 + IF(V_R)}} \\
 &= Z_0 \frac{1}{\sqrt{1 + IF(V_R)}}
 \end{aligned}
 \tag{1}$$

where

$$I_F = \frac{C_V(V_R)}{C_t d}
 \tag{2}$$

is known as the inclusion factor. Under the condition $C_V \gg C_t d$, (1) can be simplified to

$$Z_e = \sqrt{\frac{L}{C_V(V_R)}},
 \tag{3}$$

where $L = L_t d$ is the inductance per unit cell.

Equation (1) is valid as long as the frequency is far below the Bragg frequency f_B , which is defined as the frequency where the period d between two varactor-diodes is equal to half of the guided wavelength λ_g . In terms of the loaded-line phase shifter parameters, the Bragg frequency [17] is

$$f_B = \frac{1}{\pi d \sqrt{L_t C_t (1 + I_F(V_R))}}.
 \tag{4}$$

To achieve a large phase shift, both L and C_V shall be large, and to obtain a large L the unloaded transmission line is of high-impedance. The capacitance $C_V(V_R)$ changes with the bias condition, and only one bias point will achieve a perfect match with the system impedance. Therefore, the phase shifter will be mismatched when tuning the phase and there will be two extreme bias points of V_{min} and V_{max} . When designing a phase shifter, the differential phase shift $\Delta\phi$ is of interest, which is defined as the phase shift between the two extreme bias points and is expressed as follows

$$\Delta\phi = \beta(V_{min}) - \beta(V_{max}).
 \tag{5}$$

In reality, an increased phase shift normally comes with increased attenuation due to mismatch and dissipation. For this reason, a phase-shift/loss FOM is introduced

$$F_{\Delta\phi} = \frac{\Delta\phi_{degree}}{L_{dB}},
 \tag{6}$$

where L_{dB} is the total loss in the phase shifter.

Varactor-diode modeling

Under normal operation, the varactor-diodes in a loaded-line phase shifter are reversed biased and, therefore, the nonlinear capacitance of the varactor is of primary interest in the model. An equivalent circuit model of the reversed bias varactor is presented in Fig. 2(a) that is composed of a series inductance (L_s), a series resistance (R_s), a parallel capacitance (C_p), and the variable junction capacitance (C_j). The model parameters can be extracted with the real and imaginary parts of the measured impedance

$$Z(V_R) = R_s + j \left(\omega L_s - \frac{1}{\omega C_V(V_R)} \right),
 \tag{7}$$

where $C_V(V_R) = C_j(V_R) + C_p$. The variable junction capacitance can be modeled by

$$C_j(V_R) = \frac{C_{j0} \phi^n}{(\phi + V_R)^n},
 \tag{8}$$

where C_{j0} is the zero bias junction capacitance of the diode, ϕ is the built-in potential, and n is the grading coefficient [18]. Equation (8) (referred to as the standard C_V model in this paper) has been demonstrated to predict the C-V characteristics of semiconductor

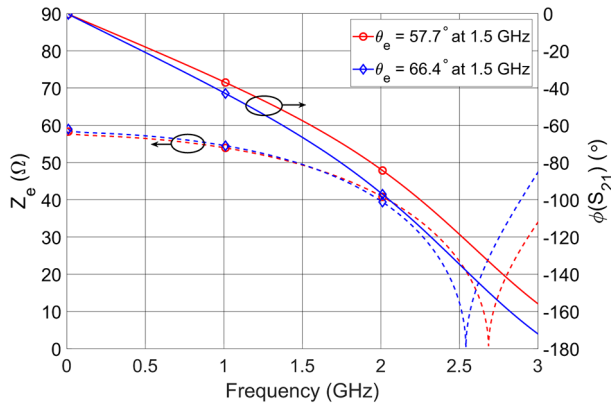


Figure 7. The simulated effective characteristic impedance and the effective electrical length for the two designed unit cells at $V_R = 5.5$ V.

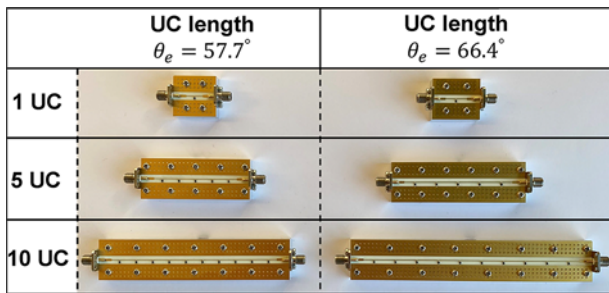


Figure 8. The fabricated phase shifters with 1, 5, and 10 unit cells.

varactors well. The model's accuracy depends on the doping profile of the p-n junction. In the case of a uniformly doped and linearly graded junction, the model has good accuracy. However, when the doping profile is highly nonuniform, the standard C_V model can have difficulty modeling the C-V characteristics. In that case, it is more suitable to model the C-V characteristics as a polynomial series expressed as

$$C_j(V_R) = C_0 + C_1 V_R + C_2 V_R^2 + \dots + C_n V_R^n, \quad (9)$$

where C_n is the polynomial coefficient of the n th-order.

Phase shifter design

Polynomial varactor model extraction

The experimental work reported in this paper is based on a hyper-abrupt varactor of model Skyworks SMV1233-079LF, chosen due to its low loss and good tuning range. Figure 2(b) depicts a two-port network utilized to extract the varactor's model parameters. The two-port network comprises a shunt varactor and two transmission lines connecting it to the input and output, forming a T-network. Hence, the varactor's impedance in (7) corresponds to Z_{12} of the two-port network. To obtain Z_{12} , the two-port network's S-parameters were measured, and the effects of the transmission lines were de-embedded. Then, Z_{12} was calculated from the de-embedded S-parameters. Two pads were employed to connect the varactor with a small amount of solder paste, and the pads and solder paste add inductance and losses. In the phase shifter simulation presented later in the paper, the varactor is directly connected from the transmission line to the ground. The contribution of the pads and solder paste is embedded in the varactor model.

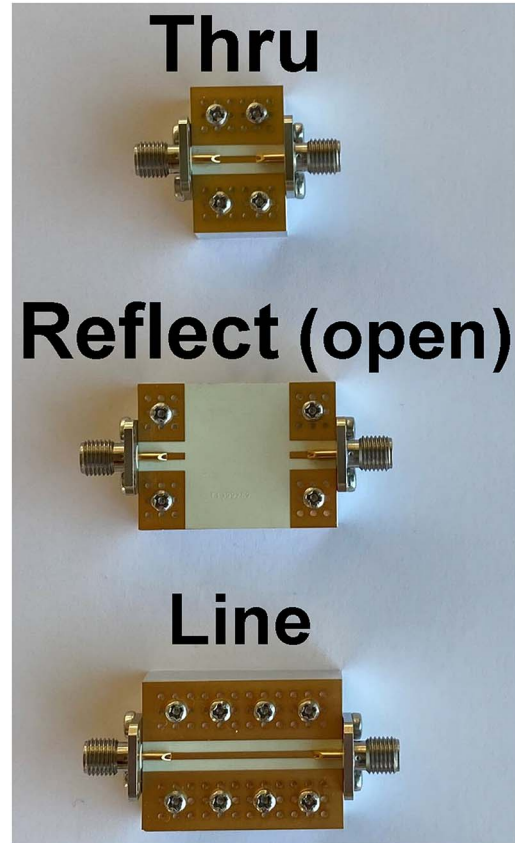


Figure 9. The fabricated thru-reflect-line circuits. The reflect is generated with an open circuit. Three lines were fabricated with line lengths of 18 mm, 83.3 mm, and 386.7 mm.

The modeled bias range of the varactor should be larger than the bias range of the phase shifter to properly model the nonlinear behavior because it has to cover the radio frequency (RF) voltage swing. Therefore, the varactor was measured for a bias range of 0.3 V to -12 V.

The C-V characteristics were obtained from the imaginary part of (7) at a low frequency of 200 MHz, where the inductor's contribution is negligible. A polynomial curve fitting of the measured C-V characteristics extracted the polynomial coefficients, which include both C_j and C_p . Table 1 presents the obtained values of the polynomial coefficients. The C-V characteristics of the measured data, the standard CV model, and the polynomial model are presented in Fig. 3. The relative error between the measurement and the two models are depicted as an inset in Fig. 3. The measured data and polynomial model have excellent agreement with a maximum relative error of 2.4%. In contrast to the polynomial model, the standard CV model has large discrepancies compared to the measured data with a maximum relative error of 9.9%. In the comparison, the standard CV model utilizes the datasheet parameters. However, even with optimization of the parameters, it was not possible to have a good agreement between the model and the measured data for the full bias range. When the C-V characteristics are not accurately modeled it will affect the accuracy of the nonlinear behavior, which will be discussed in Section V. In this work, the polynomial varactor model (9) was employed due to its superior C-V fit for highly nonuniform varactor-diodes.

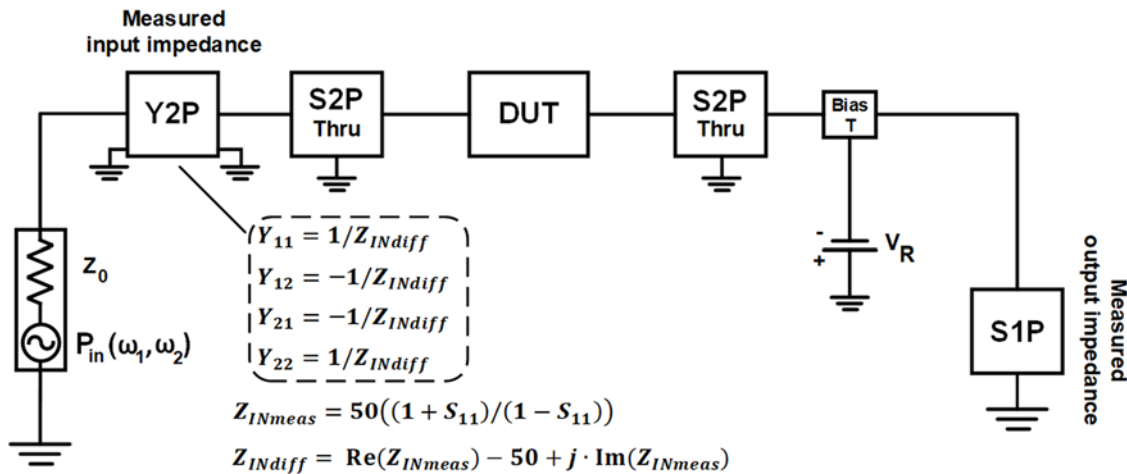


Figure 10. Illustration of the simulation setup in ADS. The input is composed of the signal generator, the measured input impedance of the measurement setup as a Y2P component, and the S2P of the thru. The output is composed of the measured output impedance of the measurement setup as an S1P, the bias setup, and the S2P of the thru. The simulated system impedance $Z_0 = 50 \Omega$.

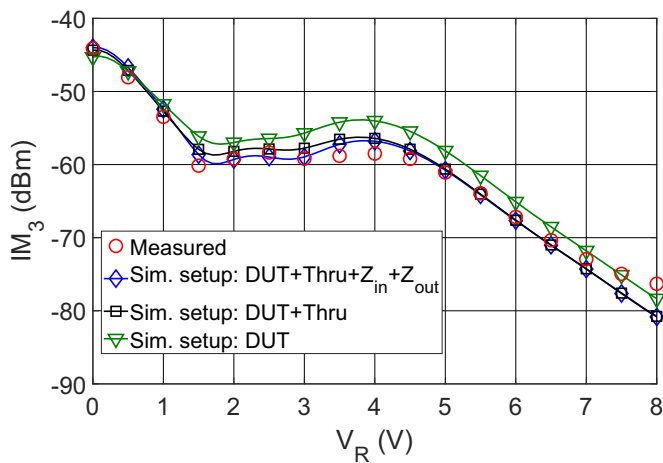


Figure 11. IM_3 for different simulation setups at 1.6 GHz with $P_{in} = 1.6$ dBm.

The series inductance was determined from the frequency-dependency of the measured C-V. From measured Z_{12} and $C_V(V_R)$ extracted at low frequency, $L_s = 1.51$ nH was obtained using a least-square fit of the imaginary part of (7) versus frequency for each bias voltage, which can be compared to the datasheet value of 0.7 nH. The larger extracted value is due to the inductance from the pads connecting the varactor. At higher frequencies, L_s has a greater influence on $Im(Z_{12})$ and to adequately model the nonlinear behavior this influence should be modeled to at least the frequency of the third harmonic. Figure 4 depicts the $Im(Z_{12})$ for the second and third harmonic, corresponding to 3 GHz and 4.5 GHz, respectively. The second harmonic is inductive at the lower range of V_R , and the third harmonic is inductive over the full range of V_R .

Lastly, the series resistance was found from $Re(Z_{12})$. The measured resistance versus bias is depicted in Fig. 5. At low frequency, the measurement is noisy, and at higher frequency the resistance increases due to the skin effect and distributed effects in the varactor. The resistance was obtained by finding the average for each frequency and then calculating the average of those averages.

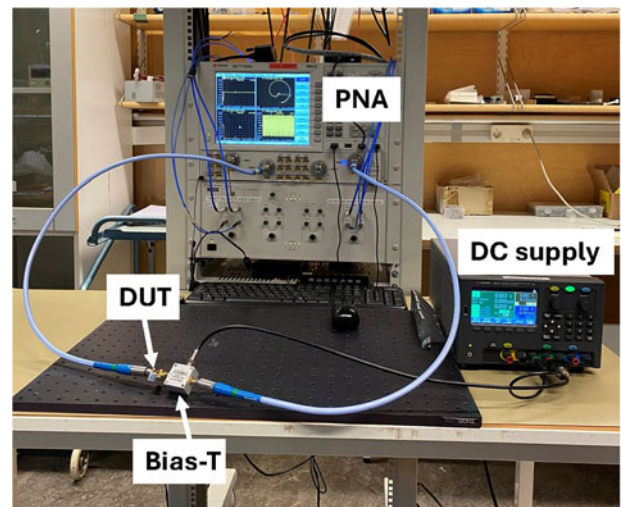


Figure 12. S-parameter measurement setup. Note that the polarity of the DC supply output is reversed to achieve a negative bias over the varactor.

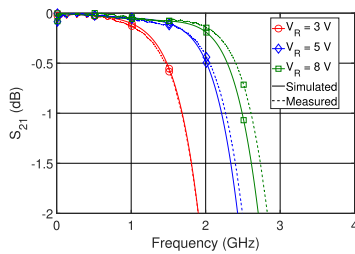
The frequencies were limited to 1.5–2.5 GHz to avoid the measurement noise, skin effect, and distributed effects at high frequencies. The obtained R_s was 1.49 Ω , which is close to the datasheet value of 1.2 Ω .

Realization of loaded-line phase shifter

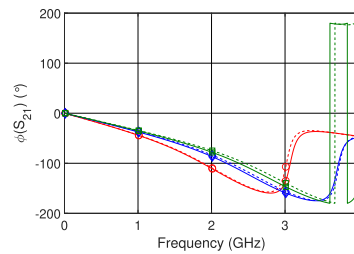
The design parameters of a loaded-line phase shifter are the loading capacitance C_0 , the unloaded impedance Z_0 , and the physical length θ_0 . The loaded-line phase shifters were designed with two different unit cells differentiated by the effective electrical length θ_e . Both unit cells have the same configuration, which is a T-unit cell that is composed of a grounded coplanar waveguide (CPWG) and a shunt varactor-diode located in the center, as illustrated in Fig. 6. The CPWG was manufactured on the substrate Rogers RO4350 with $\epsilon_r = 3.66$. The unit cells were designed to have $Z_e = 50 \Omega$ and two different θ_e at the center of the tuning range and at

Table 2. Summary of the measured $\Delta\phi$, FOM, IL, RL at 1.5 GHz, and the IIP3 at 1.6 GHz for all fabricated phase shifters. The IL is presented when $V_{Rmin} = 3$ V, which gives the largest IL. The RL is selected at $V_R = 5$ V. The IIP3 is selected at $V_R = 5.5$ V

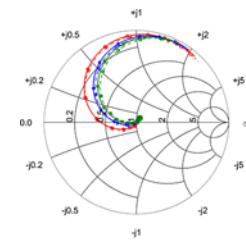
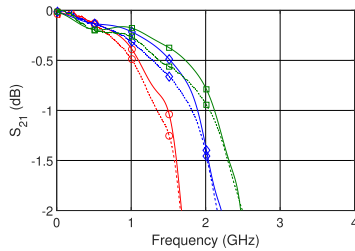
Unit cell length $\theta_e = 57.7^\circ$										
UC	$\Delta\phi$ ($^\circ$)		FOM ($^\circ/\text{dB}$)		IL (dB)		RL (dB)		IIP3 (dBm)	
	Sim.	Meas.	Sim.	Meas.	Sim.	Meas.	Sim.	Meas.	Sim.	Meas.
1	18.0	18.9	33.3	33.2	0.54	0.57	29.1	32.9	34.5	35.1
5	88.3	88.9	87.4	72.3	1.01	1.23	28.9	46.4	27.7	28.7
10	177	185	87.6	70.8	2.02	2.61	30.9	33.6	25.5	26.2
Unit cell length $\theta_e = 66.4^\circ$										
UC	$\Delta\phi$ ($^\circ$)		FOM ($^\circ/\text{dB}$)		IL (dB)		RL (dB)		IIP3 (dBm)	
	Sim.	Meas.	Sim.	Meas.	Sim.	Meas.	Sim.	Meas.	Sim.	Meas.
1	18.7	19.9	32.8	30.6	0.57	0.65	29.2	32.1	34.2	34.8
5	94.8	97.7	72.9	64.7	1.30	1.51	37.9	43.0	27.0	28.4
10	188	195	77.4	69.1	2.43	2.82	32.9	36.8	24.2	26.0



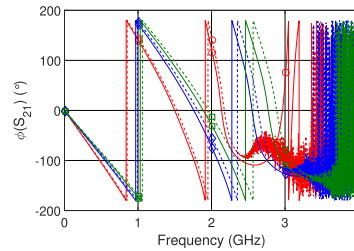
(a) IL for 1 UC.



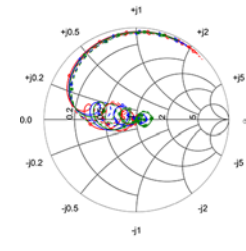
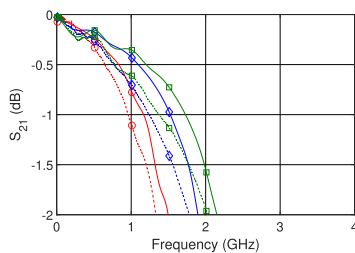
(b) Phase shift for 1 UC.

(c) S_{11} in Smith chart for 1 UC.

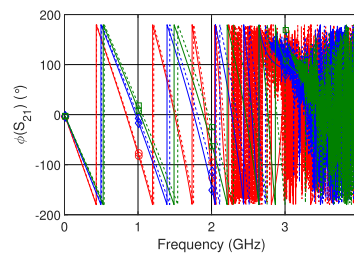
(d) IL for 5 UC.



(e) Phase shift for 5 UC.

(f) S_{11} in Smith chart for 5 UC.

(g) IL for 10 UC.



(h) Phase shift for 10 UC.

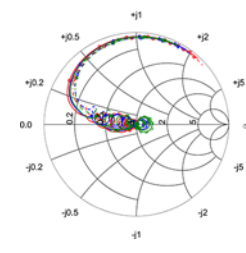
(i) S_{11} in Smith chart for 10 UC.

Figure 13. The simulated and measured S-parameter results of the realized phase shifters with a unit cell length of 57.7° .

the design frequency of 1.5 GHz. The tuning range was selected to be from $V_R = 3$ V to $V_R = 8$ V. The lower limit of V_R was selected because of two reasons. Firstly, there is a risk that the varactor becomes forward-biased when V_R is close to zero because of the addition of the RF voltage swing. Secondly, the phase shifter's insertion loss (IL) increases significantly when $V_R < 3$ V, which

makes the phase shifter unsuitable in that bias range. The upper limit was selected to avoid the breakdown region, and a larger limit only resulted in minimal gain in terms of tuning range. In Fig. 7, the simulated phase $\phi(S_{21})$ and Z_e are presented for the two unit cells at the center of the tuning range $V_R = 5.5$ V. The shorter unit cell has a $\theta_e = 57.7^\circ$ at the design frequency and a $Z_0 = 100 \Omega$.

The longer unit cell has a $\theta_e = 66.4^\circ$ at the design frequency and a $Z_0 = 90 \Omega$. All dimensions of the two unit cells are presented in Fig. 6.

With the two designed unit cells, six phase shifters were fabricated with 1, 5, and 10 unit cells, which have the purpose to validate the polynomial varactor model and to compare the FOM and linearity with respect to unit cell length and number of unit cells. The fabricated phase shifters are depicted in Fig. 8, where one can see that the input and output consist of a coaxial connector and a thru line. To de-embed the effect of the coaxial connector and the thru line, a thru-reflect-line (TRL) was designed as described in [19], and the TRL design is depicted in Fig. 9. Three lines were fabricated to cover the frequency range from 40 MHz to 4 GHz.

Nonlinear phase shifter simulations

In this paper, a harmonic balance simulation in Advanced Design System (ADS) was utilized with the diode model presented in Section III. The IM products generated in the device under test (DUT) are affected by the impedance connected to the DUT's input and output. Ideally, the measurement system presents 50Ω to the DUT from baseband to higher-order harmonics for each bias. However, this is rarely the case and, therefore, the S-parameters of the measurement setup connected to the input and output of the DUT were measured and added to the simulation setup. The measurement setup is provided in Section V. The S-parameters of the thru line connected to the DUT, shown in Fig. 6, were also added to the simulation setup. The simulation setup is illustrated in Fig. 10. The measured input impedance of the measurement setup was a 1-port S-parameter (S1P) measurement. However, the S1P was converted to a 2-port equation-based admittance (Y2P) component in ADS because of its location between the signal generator and the thru line in the simulation setup. The two fundamental tones had the frequencies of 1.5 GHz and 1.55 GHz generating the upper-band IM_3 product at 1.6 GHz. The harmonic balance mixing order was set to 5 and all S-parameters were measured up to 15 GHz, which covers well beyond the frequency range of the mixing order. Figure 11 compares the upper-band IM_3 product for different simulation setups for the unit cell with $\theta_e = 57.7^\circ$. The figure shows a noticeable difference between simulated and measured results when only the DUT is present. The greatest improvement comes from adding the measured S2P component of the thru. However, the addition of the measurement setup's impedance improves the agreement of simulated and measured IM_3 between 1.5 V and 4 V.

Experimental results

Phase shifter performance

The implemented phase shifters have been measured using a N5222A PNA Microwave Network Analyzer (Fig. 12) and simulated in ADS. The simulated and measured IL, phase shift, and return loss (RL) were compared to validate the polynomial varactor model. The results of the phase shifters with different unit cell lengths share similar results that are summarized in Table 2. Figure 13 depicts the IL, phase shift, and RL for the phase shifters with a unit cell length of 57.7° . The shape and trends are similar for the 66.4° phase shifter. For all phase shifters, the measured data agree well with the results from the model. The measured IL for the phase shifters with 5 and 10 unit cells are larger than the simulated

IL, which may be attributed to higher metal loss due to deviating conductivity and higher surface roughness in the fabricated phase shifters. There is also some deviation in phase shift after 2 GHz between simulated and measured results, where the phase shifter becomes more dispersive. Figure 14 depicts $\Delta\phi$ between $V_{Rmin} = 3$ V and $V_{Rmax} = 8$ V. Figure 15 depicts the FOM over frequency for V_{Rmax} . The measured result has unrealistic values at low frequency due to limited precision in vector network analyzer (VNA) calibration, which greatly impacts the low IL. The measured FOM is lower than the simulated FOM after 0.5 GHz because of the larger measured IL. Table 2 shows that the measured $\Delta\phi$ at 1.5 GHz is greater for the phase shifters with the longer unit cell length of 66.4° . This is to some extent surprising as the phase shift is expected to increase as the varactor inclusion factor increases. However, a longer unit cell is also more dispersive and the dispersion accelerates the phase shift, as can be seen in Fig. 13. The FOM is larger for the phase shifters with the shorter unit cell length of 57.7° due to lower IL. Consequently, the phase shifters with the shorter unit cell present the best performance in terms of both FOM and linearity. In Section VI, it will be investigated how the performance can be further optimized by tuning the unit cell length and adapting the varactor-capacitance value.

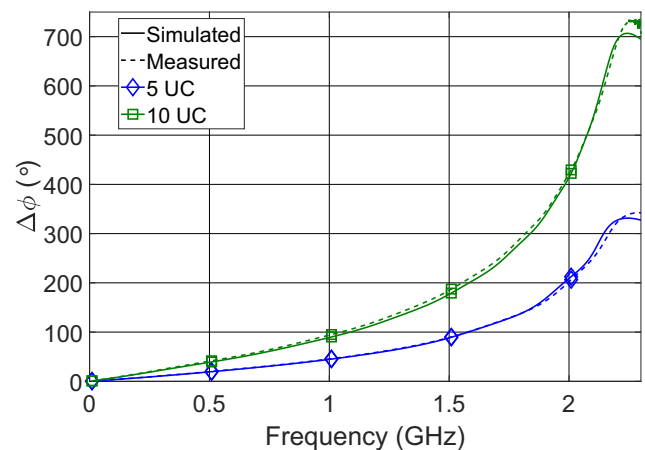


Figure 14. The differential phase shift between $V_{Rmin} = 3$ V and $V_{Rmax} = 8$ V for the phase shifters with a unit cell length of 57.7° .

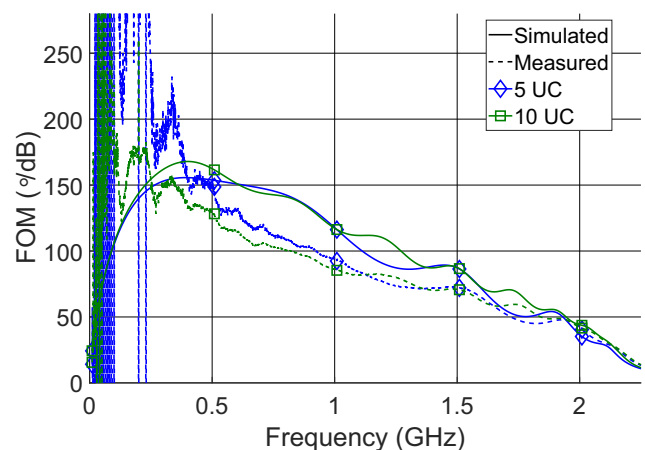
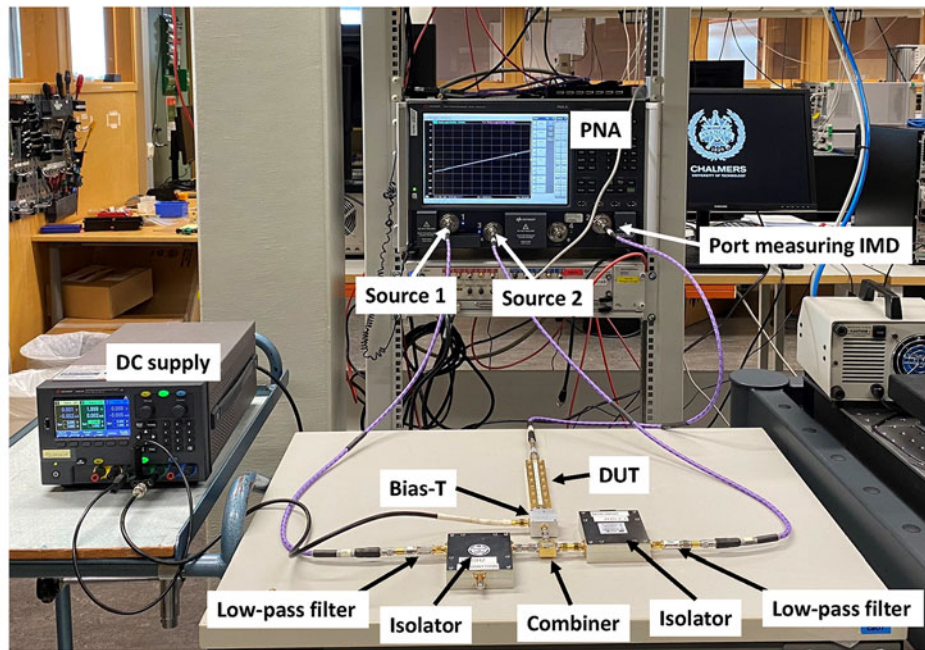
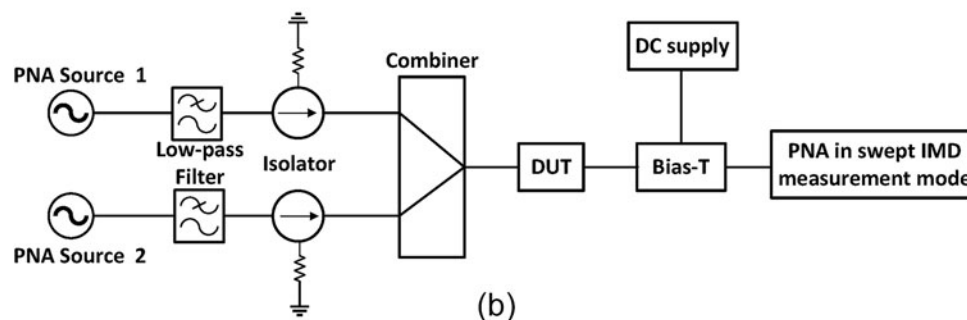


Figure 15. FOM at $V_{Rmax} = 8$ V for the phase shifters with a unit cell length of 57.7° .



(a)



(b)

Figure 16. Two-tone measurement setup for forward IM (a) measurement setup (b) illustration. The fundamental signals are generated by the PNA internally, and the IM is measured with the same PNA at a third port in swept IMD measurement mode.

Phase shifter IMD

To examine the linearity of the fabricated loaded-line phase shifters a two-tone measurement was carried out, and the measurement setup is shown in Fig. 16. The measurement was performed with a network analyzer Keysight PNA-X N5247B (PNA) that both generated the two fundamental signals and measured the IM with the swept IMD measurement type enabled. Two sources generate the two fundamental signals internally of the PNA, and the two signals exit two different ports. Each channel is connected to a low-pass filter (DC-2250 MHz) to suppress any harmonics generated in the sources. The low-pass filter is connected to an isolator to prevent leakage between the channels and to suppress any reflections. After the isolators, the two signals are combined in a 6-dB combiner that is connected to a bias-T, which is connected to the DUT. The DUT is then connected to a third PNA port that measures the IM generated in the DUT. The measurement setup's noise floor was measured to -115 dBm, and the residual IM was below this level.

The IM_3 was simulated and measured with an input power swept from -18 dBm to 1.6 dBm. A comparison of the phase

shifters' linearity is presented in Table 2 in terms of the IIP_3 . The IIP_3 was obtained by extrapolating the measured input power and IM_3 . With more unit cells the phase shifters become more nonlinear and the IIP_3 decreases. The results also show that the phase shifters with a shorter unit cell length have better linearity. Figure 17 shows the IM_3 as a function of V_R at 1.6 GHz, with a P_{in} of 1.6 dBm. The model accurately predicts the nonlinear behavior, particularly for the phase shifters with a single unit cell. There are some discrepancies between the model and the measurements for the phase shifters with 5 and 10 unit cells in the range of 3–5 V. At $V_R = 0$ V, the IM_3 has a maximum for a single unit cell whereas the phase shifters with 5 and 10 unit cells have a minimum. The minimum is attributed to suppression of the input signals because the measured $IL > 70$ dB at 1.5 GHz when $V_R = 0$ V. For a single unit cell with $\theta_e = 57.7^\circ$, the measured IL is 12.9 dB. Also, Fig. 17 presents the IM_3 for the standard C_V model for 1 unit cell. The result shows that the standard C_V model cannot properly model the nonlinear behavior of the hyperabrupt varactor. The disagreement becomes more distinct with more unit cells added.

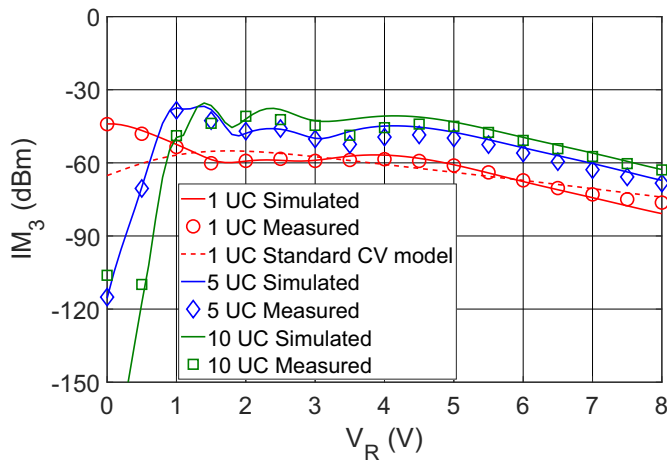


Figure 17. The IM_3 for the phase shifters with unit cell length 57.7° at 1.6 GHz with a $P_{in} = 1.6$ dBm.

Model based optimization

The main purpose of this paper is to investigate whether there is an optimum design of loaded-line phase shifters with respect to both FOM and linearity. The experiments presented in Section V revealed that a shorter unit cell is better in terms of both phase shift and linearity. In this section, it will be investigated if the performance can be further improved by optimizing the unit cell and the varactor-capacitance value. The investigation is based on the developed model with model parameters extended outside the scope of the experimental demonstrators presented above. The unit cell with a $\theta_e = 57.7^\circ$ was utilized as a reference in this study, where C_V , θ_0 , R_s , and L_s refer to that unit cell. The results are from simulations, and therefore, the simulated results of the reference unit cell are utilized.

Influence of unit cell length

The influence of the unit cell length on the phase shifter performance and linearity was investigated. The study was performed by reducing the unit cell length of the reference unit cell. The effect of reducing the unit cell length is an increased varactor-capacitance per unit cell length. To have a fair comparison, the varactor-capacitance per unit cell length was consistent for all different cases that were compared. This was achieved by modifying the varactor's capacitance with the same amount of reduction of the unit cell length. However, reducing C_V will also affect the Q factor of the varactor, and therefore, the series resistance had to be modified to compensate for the change in Q factor. Figure 18 illustrates how θ_0 , C_V , and R_s are modified with the value N . As we reduce the unit cell's length, θ_0 and C_V are divided by N , and R_s is multiplied by N . In this study, N is chosen to have the values of 1, 2, 4, and 8, where $N = 1$ for the reference unit cell. When θ_0 is divided, θ_e is not reduced with the same amount as θ_0 due to the dispersive behavior of the unit cells. Figure 19 depicts θ_e , IL, C_V , and IM_3 for the four different unit cells. The IL is greatly reduced with a shorter unit cell. The IM_3 is lowered at a larger reversed bias ($V_R > 3.5$ V) with a shorter unit cell. At a lower reversed bias, the reference unit cell has an IM_3 similar to $\theta_0/2$ and $\theta_0/4$.

The phase shift from a single unit cell is seldom sufficient for real applications. Therefore, the reference phase shifter was designed

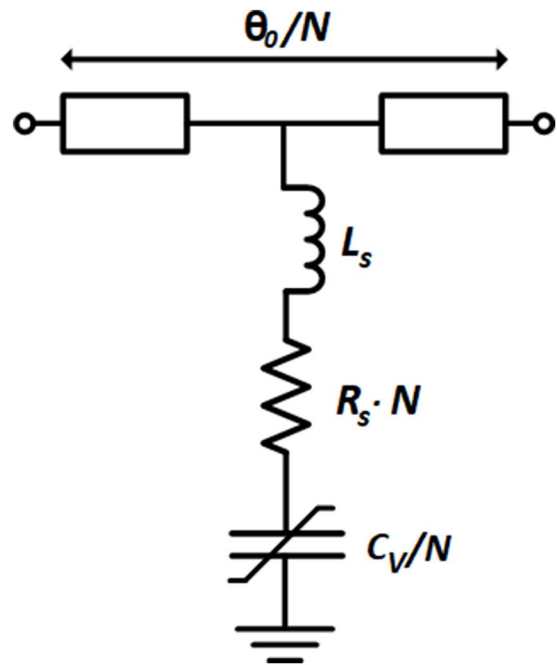


Figure 18. Modification of the unit cell to maintain the same capacitance per unit cell length and Q factor for all phase shifters. The reference unit cell has an $N = 1$. The component values are $L_s = 1.51$ nH, $R_s = 1.49$ Ω , $\theta_0 = 36^\circ$ at 1.5 GHz and $V_R = 5.5$ V, and the coefficients for C_V are shown in Table 1.

with 10 unit cells. All phase shifters had the same physical length in the investigation. To obtain the same physical length as the reference phase shifter, the phase shifters with unit cell lengths of $\theta_0/2$, $\theta_0/4$, and $\theta_0/8$ had 20, 40, and 80 unit cells, respectively. In Fig. 20, $\Delta\phi$ and FOM are presented as functions of V_{Rmin} when V_{Rmax} is set to 8 V, at the fundamental frequency of 1.5 GHz. The figure shows that if the same tuning range is utilized for all phase shifters, $\Delta\phi$ is greater with a longer unit cell, and the FOM is greater with a shorter unit cell. However, with a shorter unit cell, the IL reduces and enables a larger tuning range with a larger FOM. Therefore, Fig. 20 was utilized to find the V_{Rmin} that generated the maximum FOM for each phase shifter. The figure shows that the phase shifters with a unit cell length of θ_0 , $\theta_0/2$, $\theta_0/4$, and $\theta_0/8$, generate the largest FOM when V_{Rmin} is 3 V, 2.25 V, 2 V, and 1.75 V, respectively. In Fig. 21, the differential phase shift and FOM are depicted versus frequency when V_{Rmin} is selected to maximize FOM. It shows that the phase shifter with a unit cell length of $\theta_0/8$ has the best FOM over the majority of the frequency spectrum and achieves the largest $\Delta\phi$ from DC to 1.7 GHz. The IM_3 at 1.6 GHz is presented in Fig. 22. The lowest and highest IM_3 between the phase shifters varies with V_R . The reference phase shifter has the lowest IM_3 at low V_R , however, it obtains the largest at a V_R above 4.4 V. The phase shifters with a unit cell length of $\theta_0/4$ and $\theta_0/8$ have similar IM_3 , which is the largest at low V_R . This demonstrates that having many small nonlinear elements does not necessarily provide good linearity. The best alternative in this comparison is the phase shifter with a unit cell length of $\theta_0/2$, as it provides better linearity over the full bias range.

In summary, a phase shifter with shorter unit cells presents better phase shifter performance. In the case of IM_3 , a phase shifter with fewer longer unit cells can benefit linearity. It is a trade-off between phase shifter performance and linearity. In the comparison presented, a good trade-off would be the phase shifter with

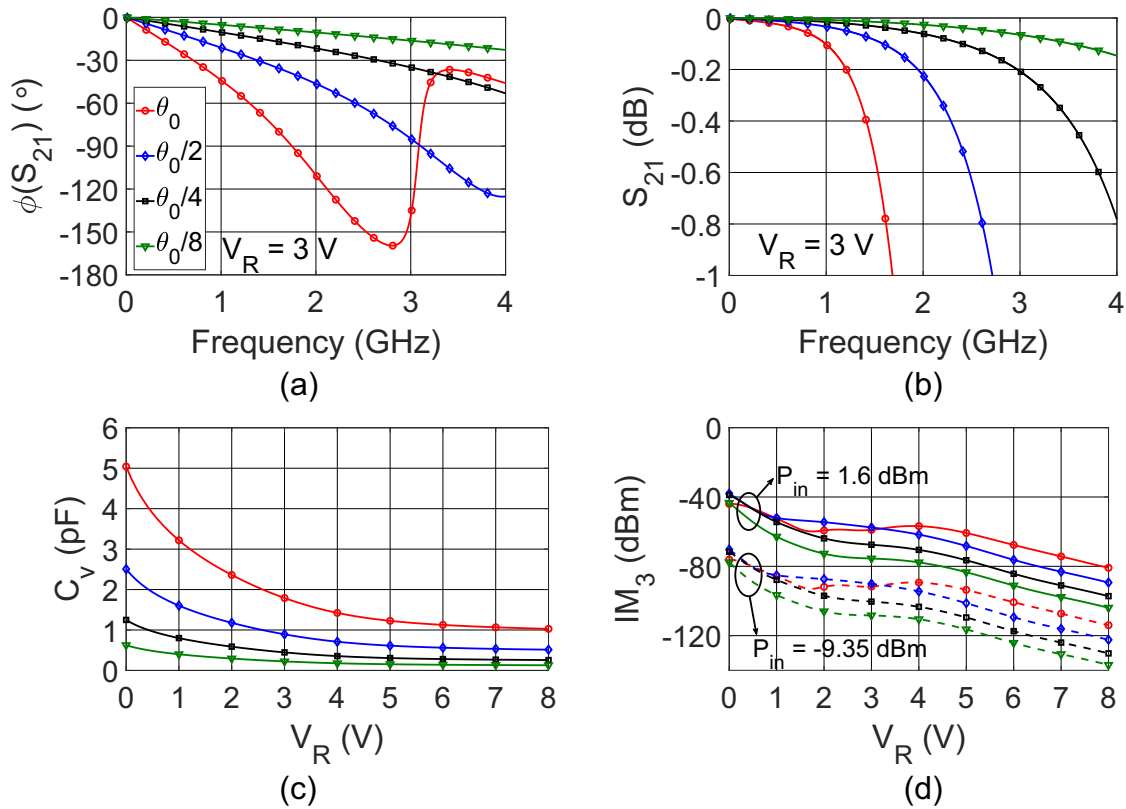


Figure 19. For each single unit cell (a) phase shift, (b) insertion loss, (c) varactor-capacitance, and (d) third-order intermodulation.

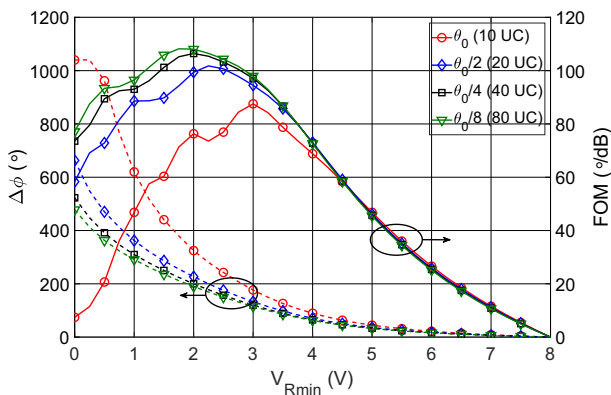


Figure 20. The differential phase and FOM at 1.5 GHz when V_{Rmin} is varied and V_{Rmax} is set to 8 V, for each phase shifter with the different unit cell lengths of θ_0 , $\theta_0/2$, $\theta_0/4$, and $\theta_0/8$. The plot shows which V_{Rmin} generates the largest FOM for each phase shifter when $V_{Rmax} = 8$ V.

a unit cell length of $\theta_0/2$ as it has good linearity over the full bias range and a $FOM = 102^\circ/\text{dB}$ at 1.5 GHz, which is close to the phase shifter with a unit cell length of $\theta_0/8$ that had a $FOM = 108^\circ/\text{dB}$.

Influence of varactor quality factor

The influence of the varactor’s Q factor on the phase shifter was investigated. The same reference unit cell was employed as in the study of the influence of unit cell length. The reference unit cell had a $Q_0 = 61$ at the design frequency of 1.5 GHz when $V_R = 5.5$ V.

The varactor’s Q factor was modified by changing R_s . Five phase shifters were compared with the Q factors of $4Q_0$, $2Q_0$, Q_0 , $Q_0/2$, and $Q_0/4$, corresponding to series resistances of $R_s/4$, $R_s/2$, R_s , $2R_s$, and $4R_s$, respectively. These five cases were investigated for a phase shifter composed of 10 unit cells. Therefore, the phase shifters have the same physical length. The Q factor affects θ_e minimally and $\Delta\phi$ is similar for all phase shifters except when they reach the cut-off region, as depicted in Fig. 23(a). When the Q factor is increased, the IL is reduced because of the reduced losses of the varactor. Therefore, the FOM is substantially increased with a larger Q factor, as depicted in Fig. 23(b). Figure 24 shows the IM_3 for the five phase shifters. The figure shows that a larger Q factor increases the IM_3 , which is attributed to the smaller series resistance. When R_s is reduced, the voltage swing over R_s is smaller and the voltage swing over C_V increases, increasing IMD. The results show that a larger Q factor greatly improves the phase shifter performance. However, it should be noted that there is a trade-off between low varactor loss and IMD.

Conclusion

In this work, it was investigated if there is an optimum design of loaded-line phase shifters with respect to FOM ($\Delta\phi_{\text{degree}}/L_{\text{dB}}$) and linearity. Six loaded-line phase shifters were implemented in PCB technology with shunt-loaded varactor-diodes. The varactor was described with an equivalent circuit, where a polynomial series was employed to model the nonlinear capacitance. It was demonstrated that the hyperabrupt varactor’s C-V characteristics must be modeled with high accuracy to predict the nonlinear behavior. Further, it was demonstrated that a careful de-embedding

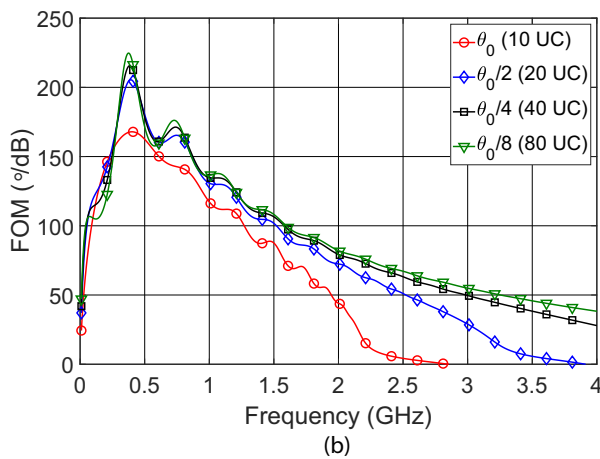
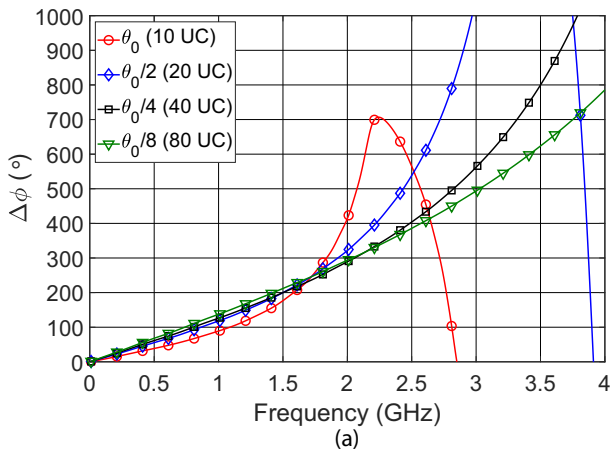


Figure 21. (a) Differential phase and (b) FOM when V_{Rmin} is selected to generate maximum FOM for each phase shifter with the different unit cell lengths of θ_0 , $\theta_0/2$, $\theta_0/4$, and $\theta_0/8$.

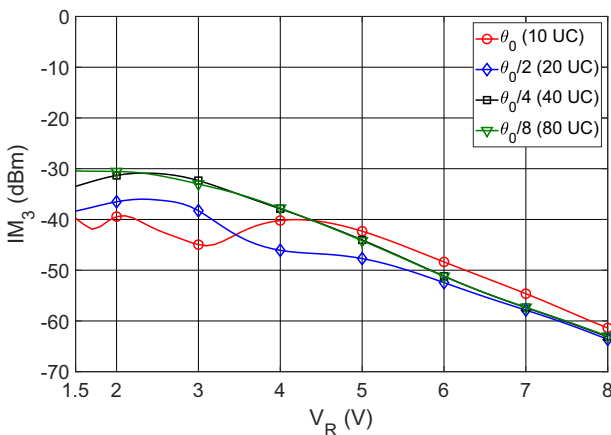


Figure 22. IM_3 for each phase shifter with the different unit cell lengths of θ_0 , $\theta_0/2$, $\theta_0/4$, and $\theta_0/8$ at 1.6 GHz with a $P_{in} = 1.6$ dBm.

of parasitic inductance of the varactor is very critical to reach good accuracy over frequency. The six loaded-line phase shifters were realized to validate the varactor model and to study the performance of the loaded-line phase shifter with varying unit cell lengths and number of unit cells. To further extend the range of

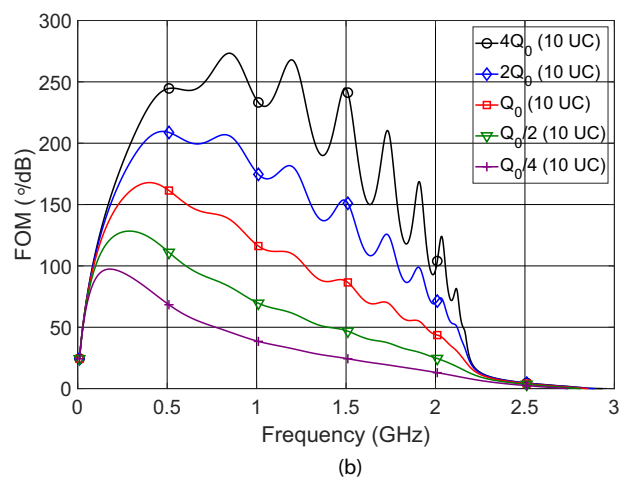
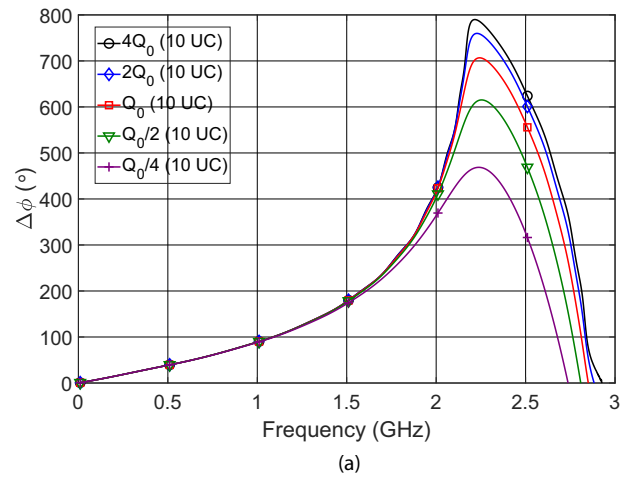


Figure 23. (a) Differential phase shift and (b) FOM for different Q factors.

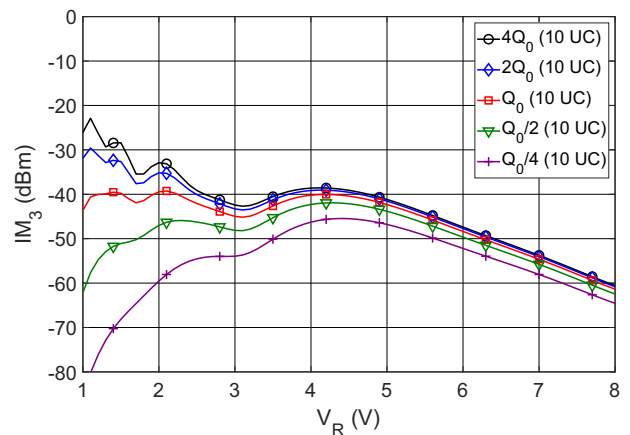


Figure 24. IM_3 for different Q factors at 1.6 GHz with a $P_{in} = 1.6$ dBm.

model parameters that affect the FOM and linearity, a simulation study was performed, based on the developed model.

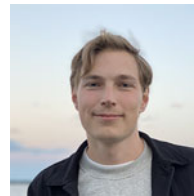
Experimental data and models demonstrate that the IMD is proportional to the varactor-capacitance per unit cell, provided that the unit cell is electrically short. If the unit cell length is increased, IMD can change due to increased dispersion. It is found that there is an optimum length where a minimum dispersion is

reached. In this study, that minimum was found to occur for an effective unit cell length about $\theta_e = 30^\circ$, however it should be emphasized that the exact value depends on the technology that determines the characteristic impedance of the transmission lines. The model also reveals that phase shifter FOM is negatively affected by dispersion when the unit cells become electrically long and that the optimum value with respect to IMD is short enough to yield a good FOM. Nevertheless, there is a trade-off between IMD and FOM since the former degrades with Q factor while the latter increases.

Competing interests. The authors declare none.

References

1. **Yang C-KK** (2003) Delay-locked loops – An overview. *Phase-Locking in High-Performance Systems: From Devices to Architectures*. New York: Wiley-IEEE Press, pp. 13–22.
2. **Lin C-S, Chang S-F, Chang C-C and Shu Y-H** (2007) Design of a reflection-type phase shifter with wide relative phase shift and constant insertion loss. *IEEE Transactions on Microwave Theory and Techniques* **55**(9), 1862–1868.
3. **Lin C-S, Chang S-F and Hsiao W-C** (2008) A full-360° reflection-type phase shifter with constant insertion loss. *IEEE Microwave and Wireless Components Letters* **18**(2), 106–108.
4. **Miyaguchi K, Hieda M, Nakahara K, Kurusu H, Nii M, Kasahara M, Takagi T and Urasaki S** (2001) An ultra-broad-band reflection-type phase-shifter MMIC with series and parallel LC circuits. *IEEE Transactions on Microwave Theory and Techniques* **49**(12), 2446–2452.
5. **Atwater HA** (1985) Circuit design of the loaded-line phase shifter. *IEEE Transactions on Microwave Theory and Techniques* **33**(7), 626–634.
6. **Nagra A and York R** (1999) Distributed analog phase shifters with low insertion loss. *IEEE Transactions on Microwave Theory and Techniques* **47**(9), 1705–1711.
7. **Mattsson M and D Kuylenstierna** (2021), “Multi-source intermodulation in a loaded-line phase shifter,” In *2020 50th European Microwave Conference (EuMC)*, Utrecht, Netherlands, 2021, pp. 280–283.
8. **Mattsson M** (2023) Intermodulation distortion in active and passive components. *LIC Dissertation* Gothenburg, Sweden: Chalmers University of Technology.
9. **Chiu H-C, Chen C-M, Chang L-C and Kao H-L** (2021) A 5-bit X-band GaN HEMT-based phase shifter. *Electronics* **10**(6), 658.
10. **Kuylenstierna D, Vorobiev A, Linner P and Gevorgian S** (2006) Composite right/left handed transmission line phase shifter using ferroelectric varactors. *IEEE Microwave and Wireless Components Letters* **16**(4), 167–169.
11. **Kuylenstierna D, Vorobiev A, Linner P and Gevorgian S** (2005) Ultrawide-band tunable true-time delay lines using ferroelectric varactors. *IEEE Transactions on Microwave Theory and Techniques* **53**(6), 2164–2170.
12. **Sandrin W** (1973) Spatial distribution of intermodulation products in active phased array antennas. *IEEE Transactions on Antennas and Propagation* **21**(6), 864–868.
13. **Kim D and Kenny JS** (2005) Experimental investigations of intermodulation distortion in tunable ferroelectric phase shifters. *IEICE Transactions on Electronics* **88**(12), 2310–2315.
14. **Dey S and Koul SK** (2014) Design, development and characterization of an X-band 5 bit DMTL phase shifter using an inline MEMS bridge and MAM capacitors. *Journal of Micromechanics and Microengineering* **24**(9), 095007.
15. **Anjos EVP, Schreurs D, Vandenbosch GAE and Geurts M** (2020) Variable-phase all-pass network synthesis and its application to a 14–54 GHz multiband continuous-tune phase shifter in silicon. *IEEE Transactions on Microwave Theory and Techniques* **68**(8), 3480–3496.
16. **Buisman K, Huang C, Zampardi PJ and de Vreede LCN** (2012) RF power insensitive varactors. *IEEE Microwave and Wireless Components Letters* **22**(8), 418–420.
17. **Rodwell M, Kamegawa M, Yu R, Case M, Carman E and Giboney K** (1991) GaAs nonlinear transmission lines for picosecond pulse generation and millimeter-wave sampling. *IEEE Transactions on Microwave Theory and Techniques* **39**(7), 1194–1204.
18. **Maas SA** (1988) *Nonlinear Microwave Circuits*. Norwood, MA: Artech House.
19. **Engen G and Hoer C** (1979) Thru-reflect-line: An improved technique for calibrating the dual six-port automatic network analyzer. *IEEE Transactions on Microwave Theory and Techniques* **27**(12), 987–993.



Martin Mattsson received the B.Sc. and M.Sc. degrees in electrical engineering and electromagnetic engineering from the KTH Royal Institute of Technology, Stockholm, Sweden, in 2018. He is currently pursuing the Ph.D. degree with the Chalmers University of Technology, Gothenburg, Sweden. His research interests include characterization and modeling of nonlinear effects of microwave hardware and passive intermodulation.



Koen Buisman (Senior Member, IEEE) received the M.Sc. and Ph.D. degrees in microelectronics from Delft University of Technology, Delft, The Netherlands, in 2004 and 2011, respectively. From 2004 to 2014, he was with the Delft Institute of Microsystems and Nanoelectronics, Delft University of Technology. In 2014, he joined the Chalmers University of Technology, Gothenburg, Sweden, where he is currently an Affiliated Associate Professor with the Microwave

Electronics Laboratory, Department of Microtechnology and Nanoscience. In 2020, he joined the University of Surrey, Guildford, U.K., where he is currently a Reader in microwave and mm-wave electronics at the Advanced Technology Institute. He is also the Director of the Nonlinear Microwave Measurement and Modeling Laboratories, a joint University of Surrey/National Physical Laboratory. He has authored or coauthored over 90 refereed journal and conference papers. He holds one patent. His current research interests include nonlinear device characterization, technology optimization, and design of linear transceivers for wireless systems.



Dan Kuylenstierna was born in Gothenburg, Sweden, in 1976. He received the M.Sc. degree in engineering physics and the Ph.D. degree in microtechnology and nanoscience from the Chalmers University of Technology, Gothenburg, Sweden, in 2001 and 2007, respectively. He is currently an associate professor with the Microwave Electronics Laboratory, Department of Microtechnology and Nanoscience, Chalmers University of Technology. His research interests include the monolithic microwave integrated circuit design, reconfigurable circuits, frequency generation, and phase-noise metrology. Dr. Kuylenstierna was the recipient of the IEEE Microwave Theory and Techniques Society (IEEE MTT-S) Graduate Fellowship Award in 2005.